Inorganic Chemistry
Article
pubs.acs.org/IC

π-Bonded Dithiolene Complexes: Synthesis, Molecular Structures, Electrochemical Behavior, and Density Functional Theory Calculations

Aurélie Damas,[†] Lise-Marie Chamoreau,[†] Andrew L. Cooksy,[§] Anny Jutand,*[,‡] and Hani Amouri*[,†]

[†]UPMC Université Paris 06, Institut Parisien de Chimie Moléculaire (UMR CNRS 7201), 4 place Jussieu, C. 42, 75252 Paris Cedex 05, France

[‡]Ecole Normale Supérieure, Département de Chimie, UMR CNRS-ENS-UPMC 8640, 24 rue Lhomond, 75231 Paris Cedex 05, France

[§]Department of Chemistry and Biochemistry, San Diego State University, 5500 Campanile Drive, San Diego, California 92182-1030, United States

Supporting Information

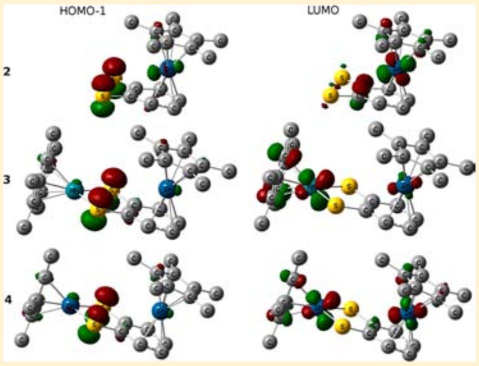

ABSTRACT: The synthesis and X-ray molecular structure of the first metal-stabilized *o*-dithiobenzoquinone [Cp*Ir-*o*-(η^4-$C_6H_4S_2$)] (**2**) are described. The presence of the metal stabilizes this elusive intermediate by π coordination and increases the nucleophilic character of the sulfur atoms. Indeed, the π-bonded dithiolene complex **2** was found to react with the organometallic solvated species [Cp*M(acetone)$_3$][OTf]$_2$ (M = Rh, Ir) to give a unique class of binuclear dithiolene compounds [Cp*Ir($C_6H_4S_2$)MCp*][OTf]$_2$ [M = Rh (**3**), Ir (**4**)] in which the elusive dithiolene η-$C_6H_4S_2$ acts as a bridging ligand toward the two Cp*M moieties. The electrochemical behavior of all complexes was investigated and provided us with valuable information about their redox properties. Density functional theory (DFT) calculations on the π-bonded dithiobenzoquinone ligand and related bimetallic systems show that the presence of Cp*M at the arene system of the dithiolene ligand increases the stability compared to the known monomeric species [Cp*Ir-*o*-($C_6H_4S_2$-κ^2-*S,S*)] and enables these complexes Cp*Ir($C_6H_4S_2$)-MCp*][OTf]$_2$ (**3** and **4**) to act as electron reservoirs. Time-dependent DFT calculations also predict the qualitative trends in the experimental UV−vis spectra and indicate that the strongest transitions arise from ligand−metal charge transfer involving primarily the HOMO−1 and LUMO. All of these compounds were fully characterized and identified by single-crystal X-ray crystallography. These results illustrate the first examples describing the coordination chemistry of the elusive *o*-dithiobenzoquinone to yield bimetallic complexes with an *o*-benzodithiolene ligand. These compounds might have important applications in the area of molecular materials.

■ INTRODUCTION

Dithiolene complexes form an important class of compounds in the area of molecular materials and have been investigated since the early 1960s by Schrauzer, Gray, and others because of their intriguing electrochemical and photophysical properties.[1] Such compounds are known to exhibit rich redox behavior imparted from the dithiolene ligands, thus allowing them to form mixed-valence compounds.[2] Indeed, a wide range of dithiolene compounds were prepared and studied by several groups and showed interesting properties.[3] For instance, Eisenberg et al. reported the synthesis and photophysical properties of several square-planar platinum bipyridyl complexes with dithiolene ligands.[4] The same group has shown that the homoleptic cobalt dithiolene complex is an active catalyst for both the electrocatalytic and photocatalytic reduction of protons in aqueous media.[5] Furthermore, Nishihara et al. reported the synthesis of dithiolene cluster complexes, where the sulfur atoms of the benzenehexathiolato ligand connect several metal centers. These compounds exhibited intense electronic communication among three dithiolene units in mixed-valence states.[6]

We anticipated that a π complex of dithiobenzoquinone could be an interesting synthon or metalated dithiolene ligand to construct multimetallic species where the electronic properties of the dithiolene unit are tuned by π complexation to a Cp*Ir organometallic moiety. However, unlike benzoquinones, very little is known about the related dithiobenzoquinone.[7] The sulfur analogues are highly reactive owing to their instability, making their handling and isolation in pure form a difficult task. Thus, examples of isolated thioquinones (ortho and para) are scarce and have been generated and characterized spectroscopically only at low temperature (10 K) in an argon matrix because the compounds are extremely reactive and

Received: October 1, 2012
Published: January 17, 2013

decompose in an unknown manner upon moderate warming of the matrix.[8] The isomeric *o*-dithiobenzoquinone (1) has proven to be even more elusive than *p*-dithiobenzoquinone. Three attempts to generate this compound have been reported. (i) The matrix-isolated product from pyrolysis of 1,3-benzodithiol-2-one showed an ultraviolet spectrum suggestive of the transient benzodithiete rather than that expected of **1**.[9] (ii) Photolysis of the same starting material 1,3-benzodithiol-2-one also did not afford **1** as an isolable product, but its transient generation was proven by trapping it with dimethyl acetylenedicarboxylate to give 2,3-bis(carbomethoxy)-1,4-benzodithiin in modest yield.[10] (iii) Finally, Perkin and Green's diaminodithioquinone approach did not yield the elusive monomeric dithione **1** either; instead, a polymeric species featuring disulfide bonds was proposed.[11] All of these procedures illustrate the difficulty in isolating and stabilizing **1**.

Our group has a long-standing record in using the Cp*Ir fragment as a stabilizing entity to isolate reactive intermediates.[12] For instance, in 1998 we reported the synthesis of the first stable *o*-quinone methide metal complex, in which Cp*Ir is attached to the internal diene moiety through η^4 coordination.[13] Later, in 2006 we described the synthesis of the first stable iridium *p*-dithiobenzoquinone complex [Cp*Ir-*p*-(η^4-$C_6H_4S_2$)] and its X-ray molecular structure.[14] More recently, in 2010 we were able to isolate the *p*-diselenobenzoquinone compound [Cp*Ir-*p*-(η^4-$C_6H_4Se_2$)] and report its X-ray molecular structure.[15] The ortho congener [Cp*Ir-*o*-(η^4-$C_6H_4S_2$)] (**2**) was also reported, but all of our previous attempts to obtain suitable crystals for X-ray study were unsuccessful.

In this paper, we report the X-ray molecular structure of the elusive *o*-dithioquinone as an iridium complex **2** (Figure 1) and its use as a π-bonded dithiolene ligand toward noble metal molecular bricks such as [Cp*M(acetone)$_3$][OTf] (M = Rh, Ir) to give a unique class of binuclear dithiolene compounds [Cp*Ir($C_6H_4S_2$)MCp*][OTf]$_2$ [M = Rh (**3**), Ir (**4**)]. The molecular structures of these coordination assemblies are reported and show that **1** displays unusual coordination modes. The electrochemical behavior of binuclear complexes **3** and **4** was investigated and found to display several reversible waves during oxidation of the π-bonded dithiolene ligand and reduction of the metal centers, unlike the [Cp*Ir-*o*-($C_6H_4S_2$-κ^2-*S*,*S*)] compound.[16] Density functional theory (DFT) calculations were also carried out and support the experimental results. We feel that this novel class of compounds holds promise as important species in the area of molecular materials.

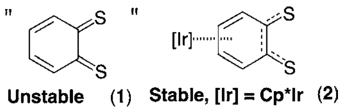

Figure 1.

■ GENERAL EXPERIMENTAL PROCEDURES

All reactions were carried out at room temperature by using standard Schlenk tube techniques. Prior to use, all solvents were dried and distilled under an argon atmosphere by standard procedures. All reagents obtained from commercial suppliers were used as received. [Cp*Ir(κ^1,κ^1-$C_6H_4S_2$)] and π-bonded dithiolene complex **2** were prepared according to literature procedures.[14b,16] All NMR data were acquired on a Bruker Avance 400 spectrometer at 400 MHz for ^{1}H NMR, 100 MHz for ^{13}C NMR, and 376 MHz for ^{19}F NMR in CD_2Cl_2. NMR chemical shifts are reported in parts per million referenced to the residual solvent proton for ^{1}H NMR and carbon for ^{13}C NMR. IR spectra were recorded on a Bruker Tensor 27 equipped with an ATR Harricks apparatus. Elemental analyses were performed by the microanalytical service of ICSN at Gif-sur-Yvette on a Perkin-Elmer 2400 apparatus.

Synthesis of {[Cp*Rh][Cp*Ir(η^6-$C_6H_4S_2$)]}{OTf}$_2$ (3). A colorless acetone solution (5 mL) of AgOTf (50.0 mg, 0.194 mmol) was added to a pink acetone suspension (5 mL) of [Cp*Rh(μ-Cl)Cl]$_2$ (30.0 mg, 0.485 mmol). The reaction mixture was stirred for 15 min and filtered through Celite, and the solvent was removed under vacuum to afford a bright-orange solid. Then, a brown acetone solution (10 mL) of **2** (45.4 mg, 0.097 mmol) was added on the previous solid, and the reaction mixture was stirred overnight. After that, the reaction mixture was evaporated to dryness, and the dark-orange solid was crystallized from MeOH/Et_2O to afford dark-orange needles (58.2 mg, 0.058 mmol). Yield: 60%. ^{1}H NMR (400 MHz, CD_2Cl_2-d_2): δ 7.62−7.64 (m, 2H, CH arene), 7.16−7.17 (m, 2H, CH arene), 2.03 (s, 15H, RhCp*), 1.89 (s, 15H, IrCp*). ^{13}C NMR (100 MHz, CD_2Cl_2-d_2): δ 136.2 (s, *Cq* arene), 103.5 (d, J_{C-Rh} = 4.9 Hz, *Cq* RhCp*), 102.1 (s, *Cq* IrCp*), 96.7 (d, J_{C-Rh} = 7.4 Hz, CH arene β-S), 92.3 (s, CH arene γ-S), 11.1 (s, CH_3 RhCp*), 8.6 (s, CH_3 IrCp*). ^{19}F NMR (376 MHz, CD_2Cl_2-d_2): δ −78.8 (s, OTf). IR (ATR): ν 3548, 3053, 2925, 1628, 1474, 1454, 1426, 1399, 1381, 1337, 1253, 1221, 1141, 1087, 1026, 887, 803, 756, 659, 633, 572, 516, 498, 455, 353, 318, 238, 210 cm^{-1}. Anal. Calcd for $C_{28}H_{34}F_6IrO_6RhS_4$ (1003.98 g·mol^{-1}): C, 33.50; H, 3.41; S, 12.78. Found: C, 33.03; H, 3.32; S, 12.15.

Synthesis of {[Cp*Ir][Cp*Ir(η^6-$C_6H_4S_2$)]}{OTf}$_2$ (4). This compound was prepared according to the procedure described for complex **3** using the following amounts: AgOTf (51.6 mg, 0.200 mmol), the precursor [Cp*Ir(μ-Cl)Cl]$_2$ (40.0 mg, 0.050 mmol) instead of [Cp*Rh(μ-Cl)Cl]$_2$, and **2** (47.0 mg, 0.100 mmol). Complex **4** was isolated as red needles (68.1 mg, 0.062 mmol). Yield: 62%. ^{1}H NMR (400 MHz, CD_2Cl_2-d_2): δ 7.92−7.93 (m, 2H, arene), 7.13−7.15 (m, 2H, arene), 2.13 (s, 15H, Cp*), 1.87 (s, 15H, Cp*). ^{13}C NMR (100 MHz, CD_2Cl_2-d_2): δ 137.7 (s, *Cq* arene), 102.3 (s, *Cq* IrCp*), 97.0 (s, *Cq* IrCp*), 96.9 (s, CH arene), 93.0 (s, CH arene), 10.8 (s, CH_3 IrCp*), 8.6 (s, CH_3 IrCp*). ^{19}F NMR (376 MHz, CD_2Cl_2-d_2): δ −78.8 (s, OTf). IR (ATR): ν 3503, 3056, 2926, 1633, 1472, 1456, 1425, 1384, 1343, 1250, 1222, 1142, 1087, 1025, 886, 801, 756, 661, 633, 572, 516, 499, 454, 381, 361, 319, 235, 204 cm^{-1}. Anal. Calcd for $C_{28}H_{34}F_6Ir_2O_6S_4$ (1093.25 g·mol^{-1}): C, 30.76; H, 3.13; S, 11.73. Found: C, 30.48; H, 3.06; S, 11.47.

General Setup for Cyclic Voltammetry. All experiments were performed under an argon atmosphere in a three-electrode cell connected to a Schlenk line. The counter electrode was a platinum wire of ca. 1 cm^2 apparent surface area; the working electrode was a glassy carbon disk electrode (*d* = 1 mm); the reference electrode was a saturated calomel electrode (SCE) separated from the solution by a bridge filled with 3 mL of degassed acetonitrile containing ^{n}Bu$_4$NBF$_4$ (0.3 M). A total 15 mL of degassed acetonitrile containing ^{n}Bu$_4$NBF$_4$ (0.3 M) was poured into the cell followed by 16.5 mg (0.015 mmol, 1 mM) of complex **4**. Cyclic voltammetry was performed first toward reduction potentials and then toward oxidation potentials, both at a scan rate of 0.5 V·s^{-1}. The scan rate was then varied from 1 to 10 V·s^{-1}. The reduction peak current of the first reduction peak R_1 (Figure 6) was measured and plotted versus the square root of the scan rate (see Figure S1 in the Supporting Information). The linear plot characterized a process only controlled by diffusion without any change of the number of electrons (two) transferred at R_1 when the scan rate was increased. In other experiments, cyclic voltammetry was similarly performed on a solution containing 15 mg (0.015 mmol, 1 mM) of complex **3** or 7.5 mg (0.015 mmol, 1 mM) of complex **2**.

X-ray Crystal Structure Determination of 2−4. A single crystal of compound **2**, **3**, or **4** was selected, mounted onto a glass fiber, and transferred under a cold nitrogen gas stream. Intensity data were collected with a Bruker Kappa CCD or a Kappa APEX2 with graphite-monochromated Mo Kα radiation. Unit cell parameter determination, data collection strategy, and integration were carried out with the *EVAL-14* or *APEX 2* suite of programs. Multiscan absorption

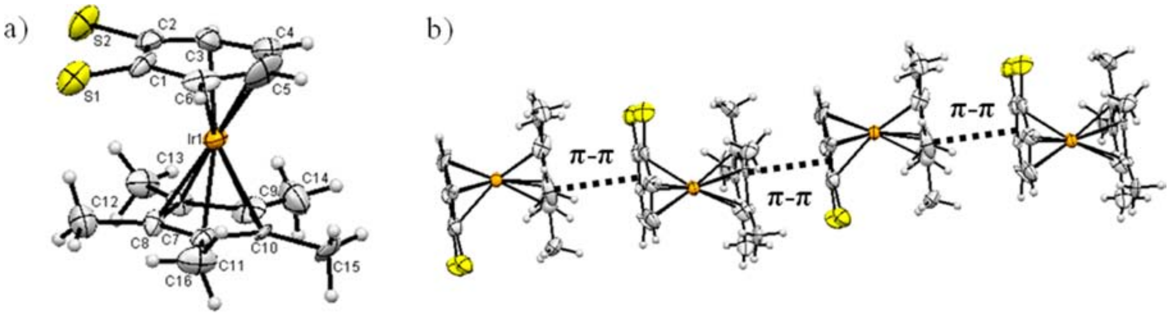

Figure 2. X-ray molecular structure of *o*-dithiobenzoquinone complex **2**: (a) molecule A with the atom numbering system; (b) π−π interaction between individual molecules.

Scheme 1

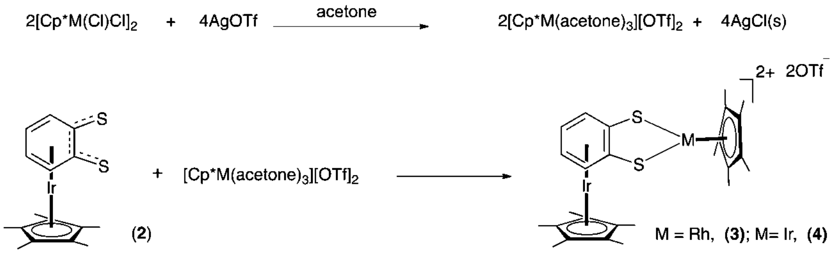

correction was applied.[34] The structures were solved by direct methods using the *SIR92* or *SUPERFLIP* programs and refined with full-matrix least squares with *SHELXL* software.[35] Almost all non-hydrogen atoms were refined anisotropically. All hydrogen atoms were placed at calculated positions.

As for complex **2**, it was difficult to select a convenient crystal for data collection. The mounted crystal was weakly diffracting and not unique; the resulting data set and crystal structure are of poor quality (R1 $[I = 2\sigma(I)] = 0.1038$). It was not possible to obtain physically reasonable atomic displacement parameters (adp's) for the C23 atom, which was thus refined isotropically. Restraints were introduced for the refinement of atom C21. The residual density is essentially located in the neighborhood of iridium atoms (about 1.1 Å from iridium atoms).

CCDC 901022 (**2**), 901023 (**3**), and 901024 (**4**) contain the supplementary crystallographic data for this paper. These data can be obtained free of charge from the Cambridge Crystallographic Data Centre via www.ccdc.cam.ac.uk/data_request/cif.

■ RESULTS AND DISCUSSION

Preparation of 2 and Its X-ray Molecular Structure. The neutral π-bonded dithiolene complex **2** was prepared as described previously by treatment of the white powder dichlorometal complex $[\mathrm{Cp^*Ir}(\eta^6\text{-}C_6H_4Cl_2)][BF_4]_2$ with an excess of dried NaSH in CH_3CN for 20 min. Compound **2** was obtained as a red microcrystalline material, analytically pure and stable under argon. After many attempts, we were finally able to obtain crystals of the *o*-dithiobenzoquinone metal complex **2** for an X-ray study, and the structure was determined. The structure of the *o*-dithiobenzoquinone **2** was confirmed by a single-crystal X-ray diffraction study. Crystals of **2** were grown by vapor diffusion of diethyl ether into a solution of the complex in CH_2Cl_2. Complex **2** crystallizes in the monoclinic system with space group $P2_1/n$ with two crystallographically independent molecules A and B.

The structure of complex **2** (Figure 2) clearly shows that the Cp*Ir moiety is coordinated to the internal four diene carbon atoms of the π-thioquinone ligand. For instance, the average value of the Ir−C bond distance to the diene subunit is 2.21(2) Å, while the Ir−C distances to the two carbon atoms in the thionyl groups are 2.47(2) and 2.51(2) Å, suggesting no interaction. Remarkably, the η^4-thioquinone ligand is planar, not bent (as one might expect) between the plane of the bonded diene part and that of the thionyl groups. This hinge angle was reported for the analogous iridium *o*-benzoquinone complex ($\theta = 4.78°$).[17] Further examination of the packing in the unit cell suggested that individual [Cp*Ir(*o*-thioquinone)] (**2**) molecules interact through π−π interactions ($d = 3.49$ Å; $\alpha = 20.9°$) between the Cp*Ir moiety and the η^4-thioquinone fragment and thus generate a 1D supramolecular chain. The C−S bond distances for the molecule are 1.71(2) and 1.72(2) Å, which is characteristic of partial double-bond character (vide infra). This bond distance is shorter than the simple C−S bond of 1.796 Å reported for 1,4-benzenedithiol[18] and slightly shorter than that of 1.766 Å for 4,4′-biphenyldithiol.[19] Overall, the solid-state structure suggests that there is some catecholate contribution for the mesomeric form of the η^4-*o*-thioquinone moiety. To our knowledge, this is the first X-ray structure of the parent *o*-thioquinone complex reported in the literature. Having elucidated its structure, we investigated the coordination properties of the chelating metal-stabilized thioquinone (**2**).

Coordination Properties of the Metal-Stabilized *o*-Thioquinone. The *o*-dithiobenzoquinone metal complex **2** was added to an orange solution of solvated $[\mathrm{Cp^*Rh(acetone)_3}][\mathrm{OTf}]_2$ prepared in situ from $[\mathrm{Cp^*Rh}(\mu\text{-Cl})\mathrm{Cl}]_2$ in acetone in the presence of AgOTf (Scheme 1). The reaction was left to proceed for several hours, and then the solvent was removed and the residue recrystallized from MeOH/Et_2O to give orange-red crystals. The new compound was fully characterized (see the experimental part) and identified as the binuclear complex **3**. Furthermore, the X-ray molecular structure of **3** was determined.

The ^{1}H NMR spectrum of **3** recorded in CD_2Cl_2 shows the presence of two doublet of doublets at δ 7.16 and 7.63 attributed to the π-bonded arene and a singlet at δ 1.89 assigned to the methyl groups of the Cp*Ir moiety. These signals are shifted downfield relative to the starting material **2**,

Table 1. Crystal and Structure Determination Data of 2−4

	2	3	4
chemical formula	$C_{17}H_{21}Cl_2IrS_2$	$C_{56}H_{70}F_{12}Ir_2O_{13}Rh_2S_8$	$C_{60}H_{80}F_{12}Ir_4O_{14}S_8$
fw	552.56	2025.82	2278.52
Z	8	4	1
T (K)	200(2)	200(2)	200(2)
wavelength (Å)	0.71073	0.71073	0.71073
cryst syst	monoclinic	monoclinic	triclinic
space group	$P2_1/n$	$P2_1/c$	$P1$
a (Å)	15.853(2)	23.030(3)	8.9356(10)
b (Å)	14.1687(12)	12.2191(15)	12.2850(19)
c (Å)	17.017(3)	24.711(2)	18.6118(17)
α (deg)	90	90	101.871(16)
β (deg)	91.915(13)	94.484(9)	99.168(10)
γ (deg)	90	90	97.776(12)
V ($Å^3$)	3820.2(9)	6932.4(14)	1943.8(4)
density calcd ($g\cdot cm^{-3}$)	1.921	1.941	1.947
cryst size (mm^3)	0.33 × 0.22 × 0.08	0.33 × 0.15 × 0.06	0.73 × 0.11 × 0.11
abs coeff (mm^{-1})	7.482	4.625	7.124
index ranges	$-22 \leq h \leq 17, -19 \leq k \leq 14, -23 \leq l \leq 18$	$-27 \leq h \leq 25, -14 \leq k \leq 10, -29 \leq l \leq 23$	$-12 \leq h \leq 12, -17 \leq k \leq 17, -26 \leq l \leq 26$
θ range	1.73−30.01	3.02−25.00	2.87−30.00
reflns collected/unique	31807/9769	32549/11972	49814/16747
final *R* indices $[I > 2\sigma(I)]$	R1 = 0.1038, wR2 = 0.2408	R1 = 0.0431, wR2 = 0.1039	R1 = 0.0403, wR2 = 0.0774
GOF on F^2	1.164	1.018	0.986
ΔF_{min} and ΔF_{max} ($e\cdot Å^3$)	6.992 and −4.664	2.856 and −2.283	2.419 and −2.111

suggesting that the dithiolene ligand adopts an *o*-dithiobenzene form. Furthermore, we note the presence of another singlet at δ 2.03, assigned to the methyl protons of the Cp*Rh moiety.

We then examined the above reaction but with the solvated iridium species $[Cp^*Ir(acetone)_3][BF_4]_2$ prepared in situ. Thus, the treatment of a light-yellow solution of the latter with 1 equiv of **2** in acetone for several hours provided an orange-red mixture from which the binuclear complex **4** was isolated following a procedure similar to that described above. The ^1H NMR spectrum of **4** recorded in CD_2Cl_2 shows the presence of two sets of doublets at δ 7.14 and 7.92 attributed to the π-bonded arene and a singlet at δ 1.87 assigned to the methyl groups of the Cp*Ir moiety. These signals are shifted downfield relative to the starting material **2**, consistent with the formation of η^6-dithiobenzene. Furthermore, we note the presence of another singlet at δ 2.13 attributed to the Cp*Ir moiety coordinated to the two sulfur atoms. Crystals of **4** for an X-ray study were conveniently obtained from a $MeOH/Et_2O$ mixture. The X-ray data for structures **2**−**4** are summarized in Table 1, and selected geometric parameters are listed in Table 2.

Red crystals of **3** and **4** were subjected to X-ray analysis. Views of the cationic parts of complexes **3** and **4** are shown in Figure 3. Complex **3** crystallizes in the monoclinic system, space group $P2_1/c$, and reveals the presence of two crystallographically independent molecules, while complex **4** crystallizes in the triclinic system, space group $P1$, also with two independent molecules. The structures of **3** and **4** show indeed that the *o*-thioquinoneiridium complex chelates the "Cp*M" (M = Rh, Ir) fragment through the two sulfur centers such that the metal center has a two-legged piano-stool geometry. Formally, the metal centers in these compounds acquire a 16-electron count and thus are unsaturated. However, the strong π-electron donation by the sulfur atoms to the metal may stabilize the electron-poor metal center. Because of this coordination mode, the aromatic ring of *o*-dithiolene is now symmetrically bound (η^6) to the Cp*Ir moiety.

Table 2. Selected Bond Lengths (Å) and Angles (deg) for 2−4[a]

		2	3	4
Bond Lengths (Å)				
C−S	C1−S1	1.71(2)	1.738(8)	1.765(10)
	C2−S2	1.72(2)	1.717(9)	1.753(9)
C−C	C1−C2	1.47(3)	1.435(11)	1.453(12)
	C2−C3	1.38(3)	1.429(12)	1.428(13)
	C3−C4	1.42(3)	1.421(14)	1.437(14)
	C4−C5	1.38(4)	1.392(13)	1.453(14)
	C5−C6	1.46(4)	1.413(12)	1.360(15)
	C6−C1	1.46(3)	1.405(11)	1.429(13)
M−S	Rh1−S1		2.265(2)	
	Rh1−S2		2.260(2)	
M−C	Ir2−S1			2.277(2)
	Ir2−S2			2.279(2)
	Ir1−C1	2.47(2)	2.316(7)	2.347(9)
	Ir1−C2	2.51(2)	2.340(7)	2.345(9)
Angles (deg)				
S−M−S	S1−Rh1−S2		89.71(8)	
	S1−Ir2−S2			89.99(8)
Cp*−M−S_2	Cp*−Rh1−S_2		88.7(2)	
	Cp*−Ir2−S_2			89.3(3)
M−S_2−S_2C_6	Rh1−S_2−S_2C_6		1.6(2)	
	Ir2−S_2−S_2C_6			2.3(1)
plane	[S1C1C2S2] and [C3C4C5C6]	2.5(3)	1.4(4)	1.6(4)

[a] With estimated standard deviations given in parentheses.

The Cp*/MS2 dihedral angles in **3** and **4** are almost perpendicular, with θ = 88.7(2)° and 89.3(3)° for **3** and **4**,

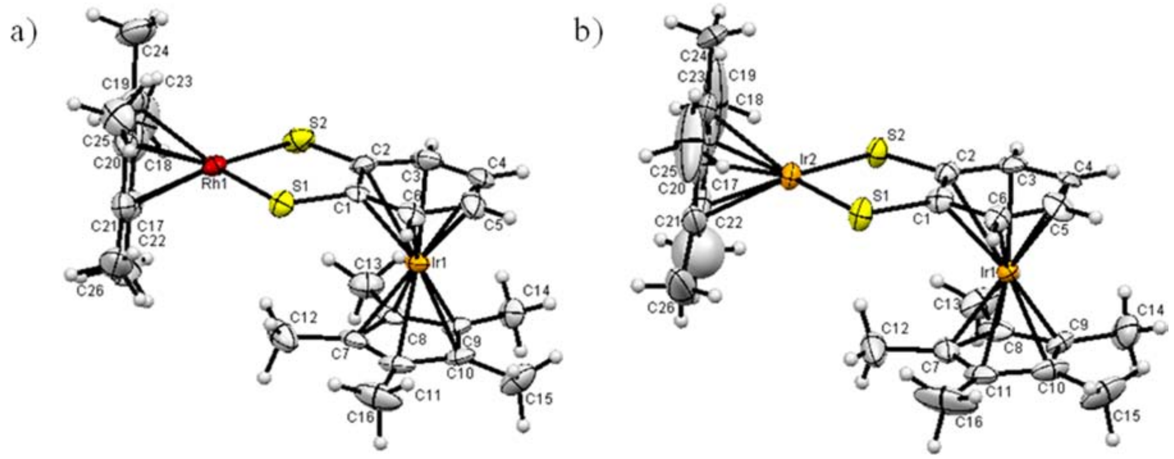

Figure 3. View of the cationic parts of complexes (a) **3** and (b) **4** with the atom numbering system.

respectively. These data compare well to those reported for monomeric complexes with thiolene ligands.[16,20]

To our knowledge, these are the first complexes featuring a π-bonded thioquinone ring that chelates a Cp*M moiety. However, we note that complexes of the type [Cp*M-(dithiolene)] were reported by the groups of Formigué and Nomura.[21]

Electrochemical Behavior of the π-Bonded Dithiolene Complexes. Cyclic voltammetry was performed at room temperature on a solution of [Cp*Ir-*o*-($C_6H_4S_2$-κ^2-*S*,*S*)] taken as the model complex in dry and degassed acetonitrile, containing ^{n}Bu$_4$NBF$_4$ (0.3 M) as the supporting electrolyte. At a steady glassy carbon disk electrode (d = 1 mm) with a scan rate of 0.5 V·s^{-1}, the iridium complex exhibited a reversible reduction peak R$_1$ ($E^p{}_{R_1}$ = −1.59 V vs SCE; E^0 = −1.56 V; Table 3) and two successive partly reversible oxidation peaks O$_1$ ($E^p{}_{O_1}$ = +0.87 V) and O$_2$ ($E^p{}_{O_2}$ = +1.22 V) (Figure 4).

Table 3. Electrochemical Data (V vs SCE) for 2–4[a]

	E (V vs SCE)				
	$E^p(O_2)$	$E^p(O_1)$	$E^p(R_1)$	$E^p(R_2)$	$\Delta E^p(O_1-R_n)$[b]
[Cp*Ir-*o*-($C_6H_4S_2$-κ^2-*S*,*S*)]	+1.218 (pr, 1e)	+0.870 (pr, 1e)	−1.596 (r, 1e)		2.466
2		+0.222 (pr, 1e)	−1.339 (r, 2e)		
3		+1.536 (pr, 1e)	−0.534 (r, 2e)	−1.447 (r, 1e)	2.983
4		+1.446 (r, 1e)	−0.562 (r, 2e)	−1.887 (r, 1e)	3.333

[a] In an acetonitrile solution with 0.3 M ^{n}Bu$_4$NBF$_4$ as the supporting electrolyte at room temperature. Scan rate = 500 mV·s^{-1}. r = reversible. pr = partially reversible. [b] n = Rh or Ir, metal of the "Cp*M^{2+}" molecular brick.

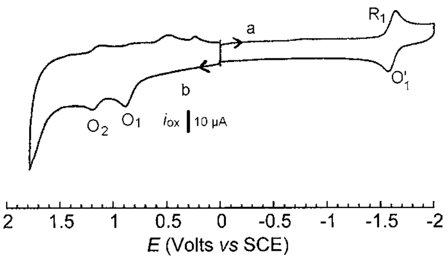

Figure 4. Cyclic voltammetry of complex [Cp*Ir-*o*-($C_6H_4S_2$-κ^2-*S*,*S*)] (1 mM) in CH_3CN containing ^{n}Bu$_4$NBF$_4$ (0.3 M) at a glassy carbon disk electrode (d = 1 mm) at a scan rate of 0.5 V·s^{-1}: (a) reduction first; (b) oxidation first. Potentials are versus SCE (oxidation peak potential of ferrocene = +0.507 vs SCE).

Scheme 2. Reduction and Oxidation of [Cp*Ir-*o*-($C_6H_4S_2$-κ^2-*S*,*S*)]

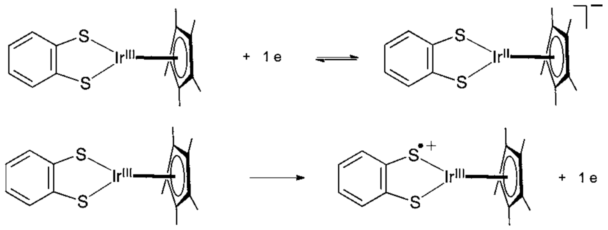

The oxidation peak current of O$_1$ and the reduction peak current at R$_1$ (reversible process) were equal. This led us to conclude that each redox process involves one electron (Scheme 2). The chemically reversible one-electron reduction indicates that the lowest unoccupied molecular orbital (LUMO) is located on the iridium(III) center whose one-electron reduction afforded an iridium(II) complex that was stable at the time scale of cyclic voltammetry (ca. 1.5 s). The highest occupied molecular orbital (HOMO) is located on the sulfur ligand. The one-electron oxidation of complex [Cp*Ir-*o*-($C_6H_4S_2$-κ^2-*S*,*S*)] at O$_1$ generated a radical cation that was not stable at the time scale of cyclic voltammetry, probably because of cleavage of the S–Ir^{III} bond in the oxidized complex.

We then investigated the electrochemistry of the π-bonded dithiolene complex **2**. Cyclic voltammetry was recorded under conditions similar to those described for the previous complex. Compound **2** exhibited one major reduction and oxidation peak but a multitude of minor reduction or oxidation peaks, evidencing that complex **2** is not very stable in solution. A main reversible two-electron reduction peak R$_1$ ($E^p{}_{R_1}$ = −1.339 V vs SCE; Table 3) and two successive partly reversible one-electron oxidation peaks at O$_1$ ($E^p{}_{O1}$ = +0.022 V) and O$_2$ ($E^p{}_{O2}$ = +0.749 V) (Figure 5) were observed.

The bielectronic reduction peak R$_1$ is assigned to reduction of the two C=S bonds of the ligand, whereas the monoelectronic oxidation peak O$_1$ is assigned to oxidation of

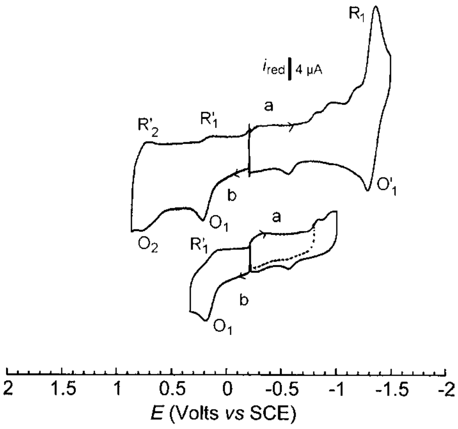

Figure 5. Cyclic voltammetry of **2** (1 mM) in CH_3CN containing $^nBu_4NBF_4$ (0.3 M) at a glassy carbon disk electrode (*d* = 1 mm) at a scan rate of 0.5 V·s^{-1}: (a) reduction first; (b) oxidation first. Potentials are versus SCE (oxidation peak potential of ferrocene = +0.507 vs SCE).

the Cp^*Ir^I moiety; see previous work on related quinone π complexes of [Cp*Ir-*p*-(η^4-$C_6H_4O_2$)].[22]

We then investigated the electrochemistry of the binuclear iridium dithiolene complex **4** compared to that of the known complex [Cp*Ir-*o*-($C_6H_4S_2$-κ^2-*S*,*S*)]. Complex **4** (1 mM) in acetonitrile exhibited, at a scan rate of 0.5 V·s^{-1}, a reversible two-electron reduction peak R_1 ($E^p{}_{R_1}$ = −0.562 V vs SCE; Table 3) followed by a second reversible one-electron reduction peak R_2 ($E^p{}_{R_2}$ = −1.887 V vs SCE; E^0 = −1.856 V; Table 3). It exhibited a reversible one-electron oxidation peak O_1 ($E^p{}_{O_1}$ = +1.455 V; E^0 = +1.414 V; Figure 6). The peak current $i_{red}(R_1)$ at the first reduction peak R_1 was plotted versus the square root of the scan rate. The linear plot in Figure S1 (Supporting Information) evidences a process controlled by diffusion. The ratio $i_{red}(R_1)/i_{red}(R_2)$ = 2 confirms a bielectronic transfer at R_1.

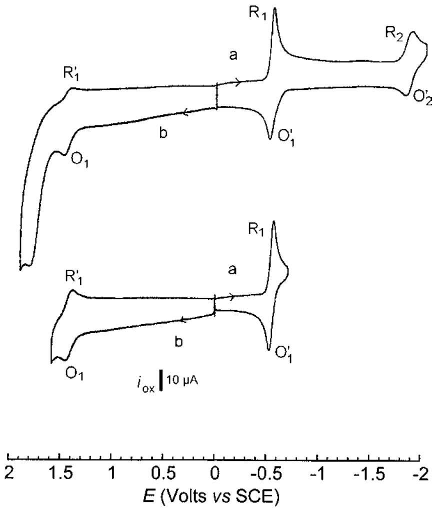

Figure 6. Cyclic voltammetry of complex **4** (1 mM) in CH_3CN containing $^nBu_4NBF_4$ (0.3 M) at a glassy carbon disk electrode (*d* = 1 mm) at a scan rate of 0.5 V·s^{-1}: (a) reduction first; (b) oxidation first. Potentials are versus SCE (oxidation peak potential of ferrocene = +0.507 vs SCE).

The reversible two-electron transfer at R_1 indicates that the LUMO of the bis-cationic iridium(III)−iridium(III) complex **4** is located on the iridium(III) ligated to the benzene ring, leading to a neutral iridium(I)−iridium(III) complex whose LUMO is located on the iridium(III) center (Scheme 3). Its further one-electron reduction at R_2 afforded an anionic iridium(I)−iridium(II) complex that was stable at the time scale of cyclic voltammetry (ca. 0.8 s). Such a complex can serve as a reservoir of electrons (Scheme 3).

The HOMO is located on the sulfur ligand. The one-electron oxidation of complex **4** at O_1 generated a complex that was stable at the time scale of cyclic voltammetry, in contrast to what was observed for complex [Cp*Ir-*o*-($C_6H_4S_2$-κ^2-*S*,*S*)] at the same time scale. The radical cation of [[Cp*Ir-*o*-($C_6H_4S_2$-κ^2-*S*,*S*)] is thus stabilized by complexation of the second iridium(III) moiety.

Finally, the electrochemistry of the heterobinuclear species **3** was studied. Complex **3** (1 mM) in acetonitrile exhibited, at a scan rate of 0.5 V·s^{-1}, a reversible two-electron reduction peak R_1 ($E^p{}_{R_1}$ = −0.544 V vs SCE; Table 3 and Figure 7) followed by a second reversible one-electron reduction peak R_2 ($E^p{}_{R_2}$ = −1.447 V vs SCE; E^0 = −1.449 V; Table 3). It exhibited a partly reversible one-electron oxidation peak O_1 ($E^p{}_{O_1}$ = +1.534 V; Figure 7). The redox properties of **3** are thus similar to those of **4**. The first reduction peak potentials of the bielectronic reduction peaks R_1 are very close. This allows us to confirm the assumption made for complex **4**, i.e., that the bielectronic reduction affects the iridium(III) ligated to the benzene ring. The second one-electron reduction at R_2 affects the rhodium(III) center. This is why the second one-electron reduction peak potentials at R_2 of **4** and **3** occur at different potential values. Indeed, this reduction process affects two different metal centers, iridium and rhodium, respectively, in the supposedly neutral complexes formed after the bielectronic reduction at R_1.

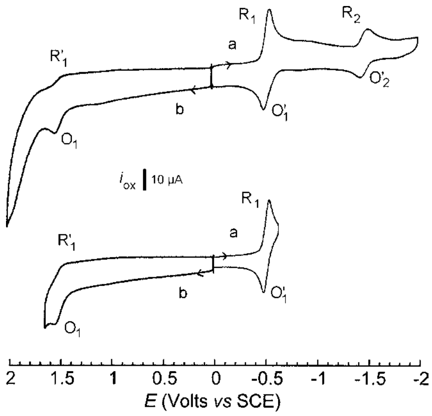

Figure 7. Cyclic voltammetry of complex **3** (1 mM) in CH_3CN containing $^nBu_4NBF_4$ (0.3 M) at a glassy carbon disk electrode (*d* = 1 mm) at a scan rate of 0.5 V·s^{-1}: (a) reduction first; (b) oxidation first. Potentials are versus SCE (oxidation peak potential of ferrocene = +0.507 vs SCE).

Thus, the HOMO is located on the sulfur ligand. The one-electron oxidation of complex **3** at O_1 generated a complex (radical cation located on one sulfur center) that was less stable than that formed in the oxidation of complex **4** at the same time scale of cyclic voltammetry (compare the reduction peak current of R'_1 on the reverse scan in Figures 6 and 7).

Scheme 3. Reduction and Oxidation of Complex 4

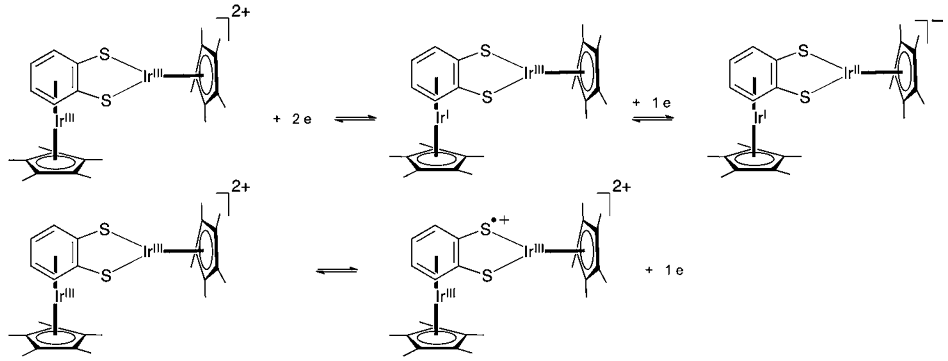

In summary, the electrochemical studies show that association of the π-bonded dithiolene complex **2** to Cp*M moieties produces a new class of stable binuclear species where electronic communication occurs between the two metal centers mediated by the dithiolene ligand. Remarkably, these compounds behave as electron reservoirs, especially complex **4**.

The UV–vis spectra of the above complexes were recorded in CH_2Cl_2 at room temperature (Figure 8). The data showed electronic absorptions (see Table 4) in agreement with a ligand-to-metal charge-transfer (LMCT)-type transition. These results indicate that the absorption energy becomes higher as follows: [Cp*Ir-*o*-($C_6H_4S_2$-κ^2-*S*,*S*)] ~ Ir–Rh (**3**) < Ir–Ir complexes (**4**).

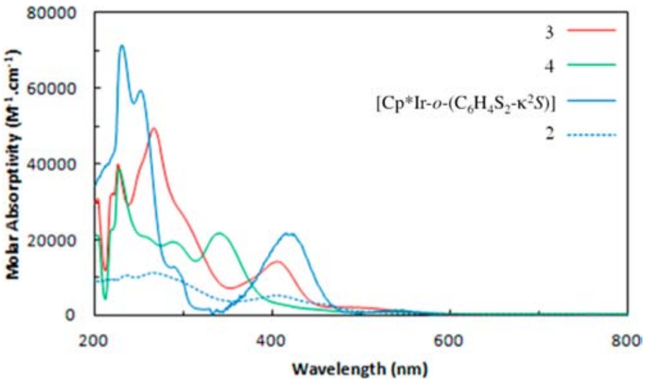

Figure 8. UV–vis spectra of complexes **2**–**4** and the model compound [Cp*Ir-*o*-($C_6H_4S_2$-κ^2-*S*,*S*)] in CH_2Cl_2.

Table 4. Electronic Absorption Maxima for 2–4 and [Cp*Ir-*o*-($C_6H_4S_2$-κ^2-*S*,*S*)]^a

	λ_{max}/nm (ε_{max}/$M^{-1}\cdot cm^{-1}$)
[Cp*Ir-*o*-($C_6H_4S_2$-κ^2-*S*,*S*)]	420 (21300)
2	406 (5290)
3	405 (14300)
4	341 (21600)

^{a}In dichloromethane at room temperature.

DFT Calculations. In an effort to support our conclusions from the structural and electrochemical studies, calculations were carried out using the B3LYP density functional.[23] The structures of **2**–**4** were optimized using the cc-pVDZ basis set[24] for the main-group atoms and the CEP-121G basis set[25] for the transition metals. Optimizations were carried out using the COSMO continuum solvation model, and time-dependent B3LYP (TD-DFT) calculations were then performed at these geometries for comparison to the observed UV–vis spectra. The initial electronic structure calculations used the *Gaussian 09* suite of programs.[26]

The TD-DFT calculations predict the spectra drawn in Figure 9, assuming a transition half-width of 0.20 eV based on the 410 nm peak of the model compound. The 30 lowest-energy transitions were modeled, and the predicted spectra effectively extended from about 250 nm to longer wavelengths. A comparison to Figure 8 shows that the calculations qualitatively reproduce the relative intensities and wavelengths of the observed peaks. The HOMO → LUMO transition in each complex is computed to lie between 530 and 580 nm, but with relatively low intensity. The longest wavelength intense peaks, predicted at 422 nm for **3** and at 381 nm for **4**, are instead primarily associated with the HOMO−1 orbital in the lower state and the LUMO in the upper state. These transitions follow the same red shift from iridium to rhodium as that observed by Nomura et al. for similar complexes.[21b]

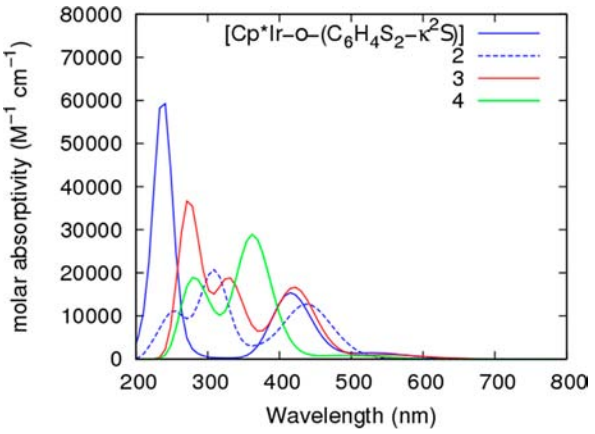

Figure 9. Computed UV–vis spectra based on TD-B3LYP/cc-pVDZ,CEP-121G/COSMO calculations.

A normal natural-bond-order analysis was used to visualize the molecular orbitals. As shown in Figure 10, the HOMO−1 in monomer **2** and in the bimetallic complexes **3** and **4** is associated with sulfur-atom p-type lone pairs, while the LUMO concentrates the electron density in the metal d orbital(s). These are the orbitals most strongly associated with the strong UV–vis transitions predicted at 448 nm (**2**), 422 nm (**3**), and 381 nm (**4**). (Other intense transitions at shorter wavelength combine LMCT character with π–π* character in the Cp*

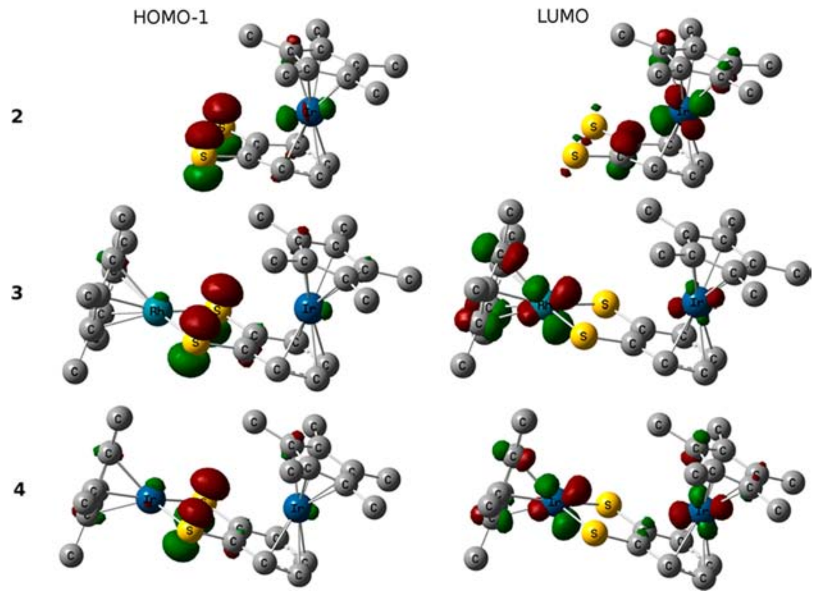

Figure 10. Plots of the HOMO−1 and LUMO for each of **2**−**4**, based on B3LYP/cc-pVDZ,CEP-121G/COSMO calculations. Hydrogen atoms are excluded for simplicity.

ring.) Like the HOMO−1, the HOMO in each species also represents the sulfur atom lone-pair density but lying in the thioquinone plane rather than perpendicular to it. These results are consistent with the electrochemical findings, predicting that the electron density shifts from the sulfur atom to the benzene-ligated iridium upon transfer from the HOMO to the LUMO. The frontier orbital analysis was extended to the uncomplexed components of **3** and **4**, finding that the HOMO and HOMO−1 in **2** still chiefly represent the sulfur-atom lone-pair density, while the LUMO in both Cp^*Rh^{2+} and Cp^*Ir^{2+} represents metal-atom d-orbital character. The bonding between the two components in each bimetallic complex may therefore be seen as mediated by mixing of the sulfur-atom lone-pair orbitals with the unfilled metal d orbitals.

To estimate the relative stability of complex **2** to the monomeric dithioquinone, we compared the energies of **2** plus three acetone molecules to those of *o*-dithioquinone plus the $Cp^*Ir(acetone)_3$ complex. We have not isolated the $Cp^*Ir(acetone)_3$ complex experimentally, but indirect evidence suggests that this is the form of Cp*Ir in solution.[27] Vibrational calculations on each structure were carried out in order to predict the free energies. Interestingly, the gas-phase calculation predicts the formation of complex **2** to be unfavorable by 21 kcal·mol^{-1}. Because interaction of the solvent with the individual species could cause substantial corrections, we applied the COSMO-RS solvent model to the gas-phase free energies. The COSMO-RS model estimates stochastic solvent effects using a relatively small number of empirically optimized parameters[28] and the charge distribution predicted by a COSMO calculation that represents the solvent using a polarizable continuum.[29] Because the COSMO-RS parameters are optimized for specific computational parameters, a BP86/TZVP[30,31] COSMO calculation of each species was first carried out using *Turbomole 6.4*.[32] On the basis of the results of these calculations, the free energy of solvation was computed using *Cosmotherm 1.05*.[33] Adding this solvation free energy to the gas-phase free energies yields an estimated free-energy change of −10 kcal·mol^{-1} for the formation of **2**, indicating that the reaction is largely driven by the favorable entropy for releasing the conplexed acetone molecules back into the solvent.

■ CONCLUSION

In conclusion, we reported the synthesis of a new series of π-bonded dithiolene complexes and their molecular structures were ascertained by single-crystal X-ray diffraction studies including the metal-stabilized reactive intermediate **2**. Electrochemical studies and DFT calculations carried out on these compounds suggest that the presence of the second metal on the arene ring increases the stability of the whole system and allows it to act as an electron reservoir. These compounds pave the way for the preparation of new complexes with important applications in molecular materials.

■ ASSOCIATED CONTENT

Ⓢ Supporting Information

X-ray crystallographic data in CIF format of **2**−**4** and reduction of complex **4**. This material is available free of charge via the Internet at http://pubs.acs.org.

■ AUTHOR INFORMATION

Corresponding Author

*E-mail: hani.amouri@upmc.fr (H.A.), Anny.Jutand@ens.fr (A.J.).

Notes

The authors declare no competing financial interest.

■ ACKNOWLEDGMENTS

We thank the CNRS, UPMC, ENS, and French ANR (Project OPTOELECTR-OM ANR-11-BS07-001-01) for supporting this work. A.L.C. thanks the NSF (Grant CHE-0947087) and ARO (Grant W911NF-10-1-0157) for equipment support.

■ REFERENCES

(1) (a) Schrauzer, G. N.; Mayweg, V. *J. Am. Chem. Soc.* **1962**, *84*, 3221. (b) Gray, H. B.; Williams, R.; Bernal, I.; Billig, E. *J. Am. Chem. Soc.* **1962**, *84*, 3596. (c) Gray, H. B.; Billig, E. *J. Am. Chem. Soc.* **1963**,

85, 2019. (d) Davison, A.; Edelstein, N.; Holm, R. H.; Maki, A. H. *Inorg. Chem.* **1963**, *2*, 1227.

(2) Eisenberg, R.; Gray, H. B. *Inorg. Chem.* **2011**, *50*, 9741.

(3) (a) Fourmigué, M. *Coord. Chem. Rev.* **1998**, *178−180*, 823. (b) Julia, F.; Jones, P. G.; Gonzales-Herrero, P. *Inorg. Chem.* **2012**, *51*, 5037. (c) Liu, W.; Wang, R.; Zhou, X.-H.; Zou, J.-L.; You, X.-Z. *Organometallics* **2008**, *27*, 126. (d) Tenn, N.; Bellec, N.; Jeannin, O.; Piekara-Sady, L.; Auban-Senzier, P.; Iniguez, J.; Canadell, E.; Lorcy, D. *J. Am. Chem. Soc.* **2009**, *131*, 16961. (e) Belo, D.; Santos, I. C.; Almeida, M. *Polyhedron* **2004**, *23*, 1351. (f) Hameau, A.; Guyon, F.; Knorr, M.; Enescu, M.; Strohmann, C. *Monatsh. Chem.* **2006**, *137*, 545. (g) Guyon, F.; Knorr, M.; Garillon, A.; Strohmann, C. *Eur. J. Inorg. Chem.* **2012**, 282. (h) Rauchfuss, T. B. *Prog. Inorg. Chem.* **2003**, *52*, 1.

(4) (a) Cummings, S. D.; Eisenberg, R. *Inorg. Chem.* **1995**, *34*, 2007. (b) Cummings, S. D.; Eisenberg, R. *J. Am. Chem. Soc.* **1996**, *118*, 1949. (c) Lazarides, T.; McCormick, T. M.; Wilson, K.; Lee, C. S.; McCamant, D. W.; Eisenberg, R. *J. Am. Chem. Soc.* **2011**, *133*, 350.

(5) McNamara, W. R.; Han, Z.; Alperin, P. J.; Brennessel, W. W.; Holland, P. L.; Eisenberg, R. *J. Am. Chem. Soc.* **2011**, *133*, 15368.

(6) (a) Shibata, Y.; Zhu, B.; Kume, S.; Nishihara, H. *Dalton Trans.* **2009**, *11*, 1939. (b) Kambe, T.; Tsukada, S.; Sakamoto, R.; Nishihara, H. *Inorg. Chem.* **2011**, *50*, 6856. (c) Tsukada, S.; Shibata, Y.; Sakamoto, R.; Kambe, T.; Ozeki, T.; Nishihara, H. *Inorg. Chem.* **2012**, *51*, 1228.

(7) Patai, S.; Rappoport, Z. *The Chemistry of the Quinonoid Compounds*, 2nd ed.; Wiley: New York, 1988.

(8) Bock, H.; Mohmand, S.; Hirabayashi, T.; Maier, G.; Reisenauer, H. P. *Chem. Ber.* **1983**, *116*, 273.

(9) Breitenstein, M.; Schulz, R.; Schweig, A. *J. Org. Chem.* **1982**, *47*, 1979.

(10) De Mayo, P.; Weedon, A. C.; Wong, G. S. K. *J. Org. Chem.* **1979**, *44*, 1977.

(11) Laksshmikantham, M. V.; Raasch, M. S.; Cava, M. P.; Bott, S. G.; Atwood, J. L. *J. Org. Chem.* **1987**, *52*, 1874.

(12) (a) Amouri, H. *Synlett* **2011**, 1357. (b) Le Bras, J.; Vaissermann, J.; Amouri, H. *Organometallics* **1996**, *15*, 5706. (c) Le Bras, J.; Vaissermann, J.; Amouri, H. *Organometallics* **1998**, *17*, 1116. (d) Le Bras, J.; Vaissermann, J.; Amouri, H. *Inorg. Chem.* **1998**, *37*, 5056. (e) Le Bras, J.; Vaissermann, J.; Amouri, H. *Organometallics* **1998**, *17*, 5850. (f) Le Bras, J.; Rager, M. N.; Besace, Y.; Vaisserman, J.; Amouri, H. *Organometallics* **1997**, *16*, 1765. (g) Le Bras, J.; Vaissermann, J.; Amouri, H. *J. Organomet. Chem.* **1998**, *567*, 57. (h) Amouri, H.; Thouvenot, R.; Gruselle, M. *C. R. Chimie* **2002**, *5*, 257. (i) Moussa, J.; Chamoreau, L.-M.; Boubekeur, K.; Rager, M. N.; Grotjahn, D. B.; Amouri, H. *Organometallics.* **2008**, *27*, 67.

(13) (a) Amouri, H.; Besace, Y.; Le Bras, J.; Vaissermann, J. *J. Am. Chem. Soc.* **1998**, *120*, 6171. (b) Amouri, H.; Vaissermann, J.; Grotjahn, D. B.; Rager, M. N. *Organometallics* **2000**, *19*, 1740. (c) Amouri, H.; Rager, M. N.; Vaissermann, J.; Grotjahn, D. B. *Organometallics* **2000**, *19*, 5143. (d) Amouri, H.; Le Bras, J. *Acc. Chem. Res.* **2002**, *35*, 501. (e) Lev, D. A.; Grotjahn, D. B.; Amouri, H. *Organometallics* **2005**, *24*, 4232.

(14) (a) Moussa, J.; Lev, D. A.; Boubekeur, K.; Rager, M. N.; Amouri, H. *Angew. Chem., Int. Ed.* **2006**, *45*, 3854. (b) Moussa, J.; Rager, M. N.; Boubekeur, K.; Amouri, H. *Eur. J. Inorg. Chem.* **2007**, 2648. (c) Moussa, J.; Amouri, H. *Angew. Chem., Int. Ed.* **2008**, *47*, 1372.

(15) Amouri, H.; Moussa, J.; Renfrew, A. K.; Dyson, P. J.; Rager, M. N.; Chamoreau, L. M. *Angew. Chem., Int. Ed.* **2010**, *49*, 7530.

(16) Xi, R.; Abe, M.; Suzuki, T.; Nishioka, T.; Isobe, K. *J. Organomet. Chem.* **1997**, *549*, 117.

(17) Moussa, J.; Rager, M. N.; Chamoreau, L.-M.; Ricard, L.; Amouri, H. *Organometallics* **2009**, *28*, 397.

(18) Ohashi, T.; Kobayashi, E.; Jinbo, T.; Furukawa, J. *J. Polym. Sci., Part A: Polym. Chem.* **1997**, *35*, 1621.

(19) Ratajczak-Sitarz, M.; Katrusiak, A.; Kaluski, Z.; Garbarczyk, J. *Acta Crystallogr.* **1987**, *C43*, 2389.

(20) Mashima, K.; Kaneyoshi, H.; Kaneko, S.; Mikami, A.; Tani, K.; Nakamura, A. *Organometallics* **1997**, *16*, 1016.

(21) (a) Nomura, M.; Fourmigué, M. *Inorg. Chem.* **2008**, *47*, 1301. (b) Nomura, M.; Tsukano, E.; Fujita-Takayama, C.; Sugiyama, T.; Kajitani, M. *J. Organomet. Chem.* **2009**, *694*, 3116. (c) Nomura, M.; Cauchy, T.; Fourmigué, M. *Coord. Chem. Rev.* **2010**, *254*, 1406.

(22) Moussa, J.; Guyard-Duhayon, C.; Herson, P.; Amouri, H.; Rager, M. N.; Jutand, A. *Organometallics* **2004**, *23*, 6231.

(23) (a) Becke, A. D. *J. Chem. Phys.* **1993**, *98*, 5648. (b) Lee, C.; Yang, W.; Parr, R. G. *Phys. Rev. B* **1988**, *37*, 785. (c) Miehlich, B.; Savin, A.; Stoll, H.; Preuss, H. *Chem. Phys. Lett.* **1989**, *157*, 200.

(24) (a) Dunning, T. H., Jr. *J. Chem. Phys.* **1989**, *90*, 1007. (b) Kendall, R. A.; Dunning, T. H., Jr.; Harrison, R. J. *J. Chem. Phys.* **1992**, *96*, 6796.

(25) Stevens, W. J.; Krauss, M.; Basch, H.; Jasien, P. G. *Can. J. Chem.* **1992**, *70*, 612.

(26) Frisch, M. J.; Trucks, G. W.; Schlegel, H. B.; Scuseria, G. E.; Robb, M. A.; Cheeseman, J. R.; Scalmani, G.; Barone, V.; Mennucci, B.; Petersson, G. A.; Nakatsuji, H.; Caricato, M.; Li, X.; Hratchian, H. P.; Izmaylov, A. F.; Bloino, J.; Zheng, G.; Sonnenberg, J. L.; Hada, M.; Ehara, M.; Toyota, K.; Fukuda, R.; Hasegawa, J.; Ishida, M.; Nakajima, T.; Honda, Y.; Kitao, O.; Nakai, H.; Vreven, T.; Montgomery, J. A., Jr.; Peralta, J. E.; Ogliaro, F.; Bearpark, M.; Heyd, J. J.; Brothers, E.; Kudin, K. N.; Staroverov, V. N.; Kobayashi, R.; Normand, J.; Raghavachari, K.; Rendell, A.; Burant, J. C.; Iyengar, S. S.; Tomasi, J.; Cossi, M.; Rega, N.; Millam, N. J.; Klene, M.; Knox, J. E.; Cross, J. B.; Bakken, V.; Adamo, C.; Jaramillo, J.; Gomperts, R.; Stratmann, R. E.; Yazyev, O.; Austin, A. J.; Cammi, R.; Pomelli, C.; Ochterski, J. W.; Martin, R. L.; Morokuma, K.; Zakrzewski, V. G.; Voth, G. A.; Salvador, P.; Dannenberg, J. J.; Dapprich, S.; Daniels, A. D.; Farkas, Ö.; Foresman, J. B.; Ortiz, J. V.; Cioslowski, J.; Fox, D. J. *Gaussian 09*, revision A.1; Gaussian, Inc.: Wallingford, CT, 2009.

(27) (a) White, C.; Thompson, S. J.; Maitlis, P. M. *J. Chem. Soc., Dalton Trans.* **1977**, 1654. (b) Amouri, H.; Guyard-Duhayon, C.; Vaissermann, J.; Rager, M. N. *Inorg. Chem.* **2002**, *41*, 1397.

(28) (a) Klamt, A. *J. Phys. Chem.* **1995**, *99*, 2224. (b) Klamt, A. *J. Phys. Chem. A* **1998**, *102*, 5074.

(29) Baldridge, K.; Klamt, A. *J. Chem. Phys.* **1997**, *106*, 6622.

(30) Perdew, J. *J. Phys. Rev. B* **1986**, *33*, 8822.

(31) (a) Schaefer, A.; Horn, H.; Ahlrichs, R. *J. Chem. Phys.* **1992**, *97*, 2571. (b) Schaefer, A.; Huber, C.; Ahlrichs, R. *J. Chem. Phys.* **1994**, *100*, 5829.

(32) *Turbomole 6.4*; University of Karlsruhe and Forschungszentrum Karlsruhe GmbH: Karlsruhe, Germany, 1989−2007.

(33) *Cosmotherm 1.05*; COSMOlogic GmbH & Co. KG: Leverkusen, Germany, 2007.

(34) (a) Duisenberg, A. J. M.; Kroon-Batenburg, L. M.; Schreurs, J. A. M. M. *J. Appl. Crystallogr.* **2003**, *36*, 220−229. (b) Blessing, R. H. *Acta Crystallogr., Sect. A* **1995**, *51*, 33.

(35) (a) Altomare, A.; Cascarano, G.; Giacovazzo, C.; Guagliardi, A.; Burla, M. C.; Polidori, G.; Camalli, M. *J. Appl. Crystallogr.* **1994**, *27*, 435. (b) Palatinus, L.; Chapuis, G. *J. Appl. Crystallogr.* **2007**, *40*, 786. (c) Sheldrick, G. M. *Acta Crystallogr., Sect. A* **2008**, *64*, 112.